Effect of interface structure on the Ru on HfO$_2$ work function

Atashi B. Mukhopadhyay · Javier Fdez Sanz ·
Charles B. Musgrave

Abstract We report an ab initio study of the effect of the
metal-*high-k* dielectric (Ru–HfO$_2$) interface structure on
the effective work function of the metal. Depending on the
structure of Ru deposited on the HfO$_2$ substrate we find a
variation of ∼0.4 eV in the effective work function of the
metal. The interfacial structures determine the extent of
charge transfer from the metal to the dielectric and hence,
affect the nature of the interface dipole. Consequently,
variability in interface structure may result in differences in
the Schottky barrier height and thus affect the electrode
work function.

Introduction

Aggressive scaling of complementary metal oxide semi-
conductor (CMOS) devices has enabled the high-speed
operation and high device density of today's integrated
circuits. However, a number of issues must be faced for
scaling beyond the sub-65-nm technology node. When the
physical thickness of SiO$_2$ is reduced below 1.5 nm, gate

A. B. Mukhopadhyay · C. B. Musgrave
Department of Chemical Engineering, Stanford University,
380 Roth Way, Stanford, CA 94305, USA
e-mail: atashi_basu@yahoo.com

C. B. Musgrave
e-mail: Charles.Musgrave@colorado.edu

J. F. Sanz (✉)
Departamento de Química Física, Facultad de Química,
University of Seville, 41012 Sevilla, Spain
e-mail: sanz@us.es

C. B. Musgrave
Department of Chemical and Biological Engineering, University
of Colorado, Boulder, CO 80309, USA

leakage current rapidly increases due to direct tunneling.
Hence, the continued scaling of MOSFETs will eventually
require replacing SiO$_2$ with a high-dielectric-constant
(high-k) material such as HfO$_2$ [1].

As the gate oxide thickness decreases, the capacitance
associated with the depleted layer at the poly-Si/gate
dielectric interface becomes significant, making it neces-
sary to consider metal gate electrodes. The search for metal
gate materials faces many challenges because the metal and
dielectric must have compatible work functions, have
chemically and thermally stable interfaces and high carrier
concentration. Ruthenium is considered a viable candidate
for PMOS because it has a vacuum work function near the
conduction band edge of Si, good thermal stability and its
oxide has low resistivity [2, 3].

Control of interfacial structure either during metal
deposition or in subsequent processing may be a critical
issue for successful application of nanoscale transistors.
During fabrication, the generation of lateral inhomogenei-
ties in the atomic structure across the interface may pro-
duce variability in electronic properties which in-turn can
affect device performance uniformity [4]. Much effort has
been exerted in optimizing metal/dielectric structures to
meet engineering requirements [5, 6]. Various experimen-
tal studies have been published within the last few years
focusing on electrical properties of Ru/HfO$_2$ systems [2, 3].
However, the structural and chemical nature of the metal/
dielectric interface has largely remained unknown due to
its intricate structure and the lack of experimental probes
for in situ atomic scale characterization of buried inter-
faces. In contrast, atomistic modeling offers microscopic
insight into otherwise inaccessible aspects of complex
interface structures.

In a previous study we investigated detailed atomistic
structures and electronic properties of Ru/HfO$_2$ interfaces

that were generated not only by epitaxial adhesion, but also by atom-by-atom deposition of Ru on HfO₂. The latter case is generally analogous to as-deposited metal films deposited by sputtering, a common method for metal deposition [12]. Our studies demonstrated that the interfacial density-of-states' properties are a sensitive function of the structure of the metal deposited. Here, we report an ab initio study that reveals that the interfacial structure of the gate metal on the gate dielectric plays a central role in determining the electronic properties of CMOS gate stacks. Among other factors, homogeneity in interface structure is a required criterion for the application of metal/high-k gate stacks in sub-65-nm CMOS technology.

The present article is organized as follows. "Computational details" section describes the computational details of this study. In "Results and discussions" section, we present and discuss results pertaining to the interfacial bonding, Schottky barrier height and work function. We finish by drawing some general conclusions in "Summary" section.
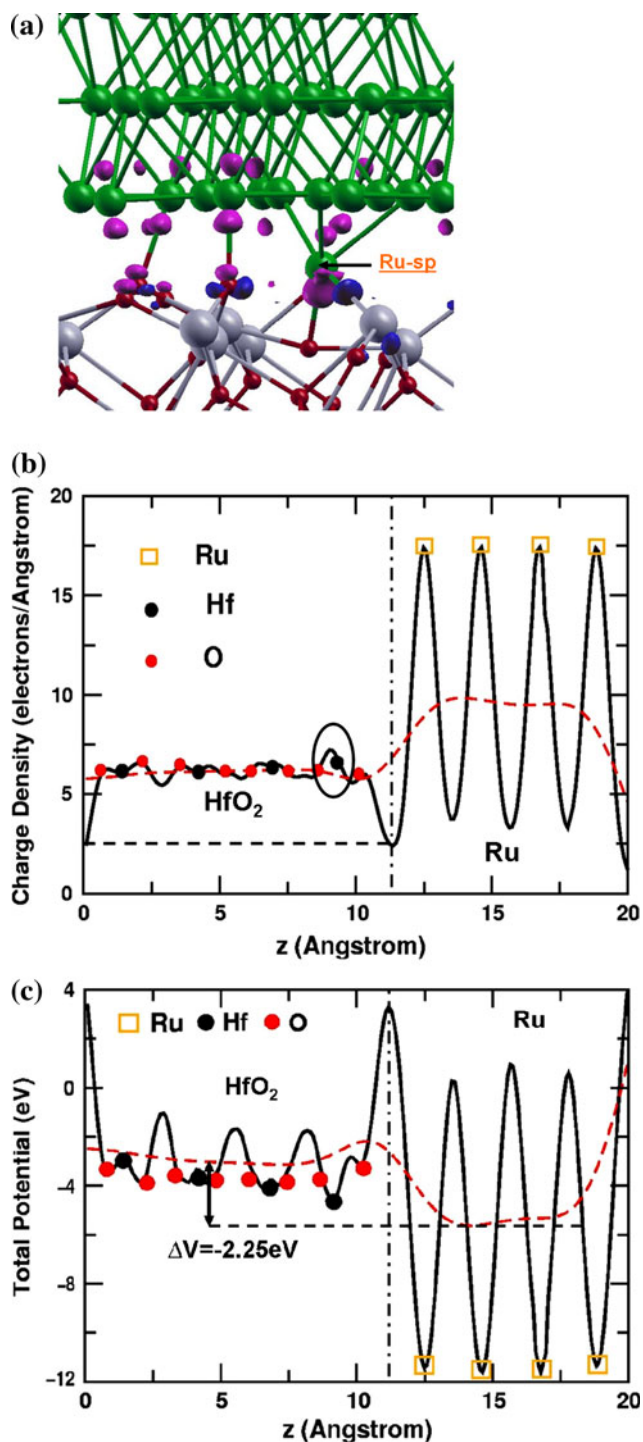
Computational details

For all calculations we used the generalized gradient approximation (GGA) to density functional theory (DFT) as implemented in the VASP code [7–9]. Specifically, we employed the PW91 GGA implementation of DFT with the electronic states expanded over a plane-wave basis set. Calculations utilized the projected augmented wave approach as applied in the VASP code. In previous work, we reported first principles studies of the structural, electronic, and thermodynamic properties of the anhydrous and hydrated low-index monoclinic HfO₂ (m-HfO₂) surfaces. Our calculations predict the bare m-HfO₂ ($\bar{1}11$) face to be the most stable anhydrous surface [10]. Although the m-HfO₂ (001) face is observed in some ALD HfO₂ films, we calculate a surface energy for m-(001) approximately 0.4 J m^{-2} larger than that of the m-($\bar{1}11$) surface suggesting that for this surface to be observed, it must be kinetically favored under certain process conditions. In fact, our ab initio thermodynamic phase diagrams of the hydrated surfaces show that the m-HfO₂ (001) face is indeed kinetically stable relative to the m-HfO₂ ($\bar{1}11$) face at typical HfO₂ ALD process conditions [11]. Thus, we chose the kinetically stable oxygen terminated (001) surface of m-HfO₂ as the dielectric substrate for Ru deposition. The valence electrons of Ru and Hf atoms as well as their semi-core electrons (4p and 5p, respectively) are explicitly treated. For O atoms 2s and 2p electrons were explicitly included. We chose a plane-wave cutoff energy of 450 eV. To model the gate electrode and dielectric interfaces we employed the well-known slab approach

consisting of a supercell that includes a portion of vacuum to model the m-HfO₂ (001) surface, a four-layered 2 × 2 supercell was used. After replication along the three lattice vectors, an array of slabs separated by vacuum was obtained. A vacuum width of 15 Å was chosen because we found it sufficient to prevent slab-to-slab interactions and to ensure convergence of the energy to within 0.001 eV/atom. For structural optimizations and investigation of electronic properties of metal/dielectric stacks, Γ-point sampling was used because the metal/dielectric supercell contained 160 atoms making the k-point sampling used for surface and bulk optimizations impractical. We have found that this approximation leads to geometries in close agreement to those obtained using k-point sampling [10].
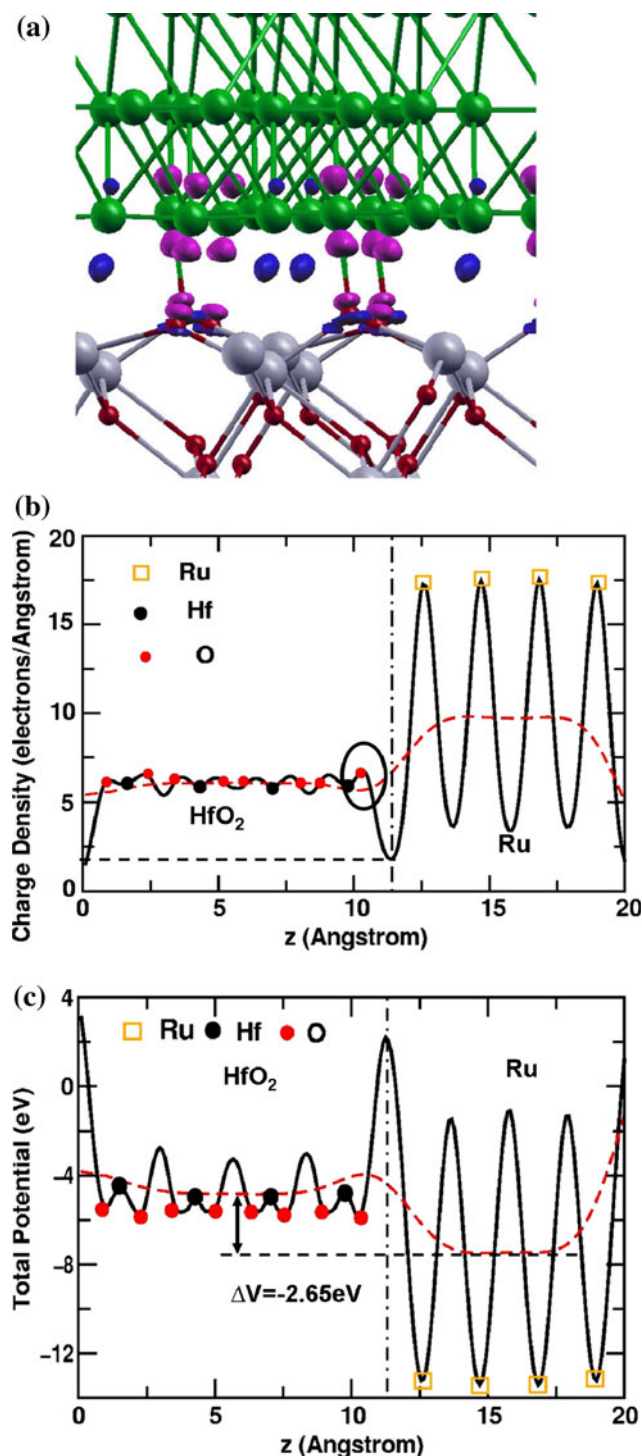
Results and discussions

Various Ru/HfO₂ interface structures were considered which consist of a four-atom layer thick film of Ru on the m-HfO₂ (001) substrate generated either by atom-by-atom (ABA) deposition or by epitaxial juxtaposition and subsequent relaxation. In the ABA case, the first two atomic layers of metal deposition were performed by adding Ru atoms one at a time to the most favorable site for adsorption with the constraint that the Ru film not exceed two atomic layers. The third and fourth layers were given a (001) close-packed structure, placed on the second layer to form A–B–A–B stacking and then relaxed. We found that the Ru/HfO₂ interface of the ABA deposited film is rougher than the epitaxially connected film. The atom-by-atom deposited film is also characterized by occupation of hollow Hf sites by Ru atoms, marked as Ru-sp in Fig. 1a (0.25 sites/2 × 2 cell), and reconstruction and reorganization of interfacial oxygen. A second kind of atom-by-atom deposited film was also considered in which the Ru atoms present at hollow Hf sites of the ABA film were removed and the structure relaxed to form the ABA1 structure. The epitaxially connected Ru film on HfO₂ was created by attaching four atomic planes of Ru atoms in A–B–A–B HCP stacking to the (001) HfO₂ surface, where the lattice mismatch of HCP (0001) Ru with m-HfO₂ (001) is approximately 7%. Again, the Ru on m-HfO₂ (001) structure was subsequently optimized. Reference [12] provides additional details about the calculations and the generation of investigated structures.

In Figs. 1a and 2a we show calculated electron density differences upon adsorption of Ru on the m-HfO₂ (100) surface for both the ABA deposited and epitaxially connected films, respectively. The regions shown in magenta lose electron density, whereas regions highlighted in blue gain electron density. In both films, Ru atoms within the bulk regions are neutral and are thus present as Ru(0).

Fig. 1 a Electron-density differences at the interface. *Gray* (*magenta*) regions lose electron density whereas *dark* (*blue*) regions gain electron density upon adsorption of Ru. Ru, O, and Hf atoms are represented by *gray* (top), *dark-small*, and *light-gray* (*green*, *red*, and *gray*) spheres, respectively, **b** plane-averaged charge-density distribution and **c** plane-averaged total potential for the ABA deposited film. The *broken lines* represent the average potential using the double-macroscopic average technique [12]. The *dotted–dashed vertical line* represents the interface. "Ru-sp" represents the Ru atom occupying the hollow hafnium site on m-HfO$_2$ (100). (Color figure online)

Fig. 2 a Electron-density differences at the interface. *Gray* (*magenta*) regions lose electron density whereas *dark* (*blue*) regions gain electron density upon adsorption of Ru. Ru, O, and Hf atoms are represented by *gray* (top), *dark-small*, and *light-gray* (*green*, *red*, and *gray*) spheres, respectively, **b** plane-averaged charge-density distribution and **c** plane-averaged total potential epitaxially connected film. The *broken lines* represent the average property using the double-macroscopic average technique [12]. The *dotted–dashed vertical line* represents the interface. (Color figure online)

However, the charge density differences at the interfacial Ru layer show a different characteristic profile. In the case of the ABA deposited film, most of the interfacial Ru atoms are oxidized. However, for the epitaxially connected film only the interfacial Ru atoms closest to interfacial oxygen atoms of the dielectric lose electron density, whereas regions with increased electron density are observed near interfacial Ru atoms further from interfacial oxygen. In both cases it can be seen that the interfacial oxygen atoms are polarized and that the bonding between the dielectric and Ru layers is predominantly ionic. However, the Ru/HfO$_2$ interface of the ABA deposited Ru film includes Ru atoms occupying hollow Hf sites on m-HfO$_2$ (100) that are marked as Ru-sp in Fig. 1a. These Ru atoms are covalently bonded to neighboring oxygen atoms of the m-HfO$_2$ (100) hollow site and thus interact strongly with the dielectric surface. Our previous analysis of the partial density of states associated with this particular Ru atom revealed the presence of distinctive s-, p-, and d- states at −16 eV, indicating mixing of Ru d orbitals with the 2s orbitals of neighboring oxygen atoms [12]. It is worth mentioning that the Ru atoms present in the epitaxially connected film are arranged in an *hcp* structure and therefore, the interface between the dielectric and metal layers is well defined. However, the Ru films formed by atom-by-atom deposition (ABA and ABA1) are found to be amorphous and to possess a relatively rough interface between the metal and dielectric, giving rise to Ru–Hf metallic bond formation. This type of hetero-metallic bonding is absent in the epitaxially connected film.

A quantitative analysis of the plane-averaged charge density distribution is presented in Figs. 1b and 2b for the ABA deposited and epitaxially connected Ru films, respectively. The charge density profile in the bulk regions of the metal and dielectric are very similar for both films, however, the profiles at the interfaces are different. The charge density localized at the interface is higher in the case of the ABA deposited film compared to the epitaxially connected film due to the presence of Ru-sp atoms at the interface. On integrating the charge density profiles over the Ru and HfO$_2$ regions we find that negligible charge transfer occurs between Ru and the dielectric region for the epitaxially connected film. However, in the case of the ABA film significant charge transfers from the interfacial Ru layer to the dielectric. We find that on average each interfacial Ru atom of the ABA deposited film loses ~0.9e, whereas interfacial Ru atoms of the epitaxially connected film loose ~0.1e on average. However, removal of Ru atoms located at hollow Hf interface sites in ABA films (resulting in the ABA1 structure) reduces the charge transfer between Ru and the HfO$_2$ dielectric film. We calculate that on average interfacial Ru atoms of the ABA1 film lose ~0.2e, indicating that Ru atoms present at hollow

Hf interface sites in the ABA deposited film are highly oxidized. For the ABA deposited film this decrease in charge density on interfacial Ru atoms can be accounted for by a concomitant increase in charge density on interfacial Hf atoms, as shown in Fig. 1a, b.

Figures 1c and 2c show the plane-averaged total potential (V) and potential lineup (ΔV) using the double-macroscopic averaging technique for both the ABA deposited and epitaxially juxtaposed Ru films, respectively [13]. The potential lineup is defined as the difference between the two plateau values of the respective bulk-like regions, i.e., sufficiently far from the interface. The p-type Schottky barrier height (SBH), ϕ_p, for these two interfaces has been calculated using the standard "bulk plus lineup" procedure [14, 15]:

$$\phi_\mathrm{p} = \Delta E_\mathrm{p} + \Delta V, \tag{1}$$

where ΔE_p is the energy difference between the metal Fermi level and the dielectric valence band maximum (VBM), each measured relative to the average total potential in the corresponding crystal. The calculated values of p-type SBHs for ABA deposited and epitaxially connected films are 2.67 and 2.30 eV, respectively. However, the ABA1 interface shows a ΔV value of 2.30 eV and a p-type SBH value of 2.62 eV. The differences between these values for the different interfaces indicate that the SBH is sensitive to interface-specific structures as shown previously both experimentally and theoretically [16]. An additional junction property is the interface dipole moment calculated from the plane-averaged charge density differences. Our estimated dipole moment across the interface for the epitaxially connected Ru film is 2.74 D. However, for the ABA deposited film, both the charge transfer and the presence of Ru–Hf bonds at the interface change the direction and magnitude of the interfacial dipole. These bonds are less polarizable and hence cause a decrease in the magnitude of the dipole moment across the interface, whose value now is −0.57 D. These changes in the interfacial dipole cause the average potential energy in the oxide layer to shift downward with respect to its value in the metal, which on the other hand increases the value of ϕ_p in the ABA deposited film model.

The *n*-type SBH, ϕ_n, was calculated using:

$$\phi_n = E_\mathrm{g} - \phi_\mathrm{p}, \tag{2}$$

where E_g is the band gap of the dielectric. The experimental band gap of 5.6 eV [16] was used rather than the DFT-GGA gap of 3.8 eV because of DFT's well-known underestimation of band gaps. The effective work function ($\phi_\mathrm{m,eff}$) of HfO$_2$ was then calculated using:

$$\phi_\mathrm{m,eff} = \phi_n - \mathrm{CBO} + \mathrm{EA}, \tag{3}$$

where CBO is the conduction band offset between the oxide and the Si substrate (2.0 eV) [17], and EA is the

electron affinity of Si (4.05 eV) [18]. The estimated values of the effective Ru work function for the ABA, ABA1, and epitaxially connected Ru films are 4.98, 5.09, and 5.35 eV, respectively. Experimentally, the work function is found to be a function of the annealing temperature with as-deposited Ru on HfO_2 having a work function of 5.1 ± 0.1 eV, which increases to 5.2 ± 0.2 and 5.3 ± 0.4 eV after forming gas anneals (FGA) of 431 and 510 °C, respectively [19]. This increase in the work function might be attributed to the conversion of amorphous ABA-like interfacial structures to more epitaxial films. However, it may also be due to various other factors not accounted for here, such as metal oxidation, annealing of defects, and interfacial mixing. We are currently investigating the effect of annealing and oxidation on the work function. However, we note that our calculated values lie within the range of reported experimental values.

Summary

In conclusion, the electronic properties of the Ru/HfO_2 interface with three dissimilar atomic structures have been investigated using GGA-based DFT simulations. From an analysis of the predicted properties we find that the structure of the interface plays a key role in determining the SBH and work function with the variation in the interfacial metal film structure on HfO_2 producing a 0.4 eV difference in the effective work function of Ru on HfO_2 for the interface structures investigated. This is consistent with the effective work functions observed for Ru on HfO_2 structures resulting from different annealing conditions. The presence of hetero-atomic Ru–Hf metallic bonds in atom-by-atom deposited films also causes changes in the dipole moment of the interface and hence decreases the effective work function. These results indicate that in order to obtain consistent electronic properties across an array of nanoscale transistors one must control the variability of the interfacial atomic structure.

References

1. Wilk GD, Wallace RM, Anthony JM (2001) J Appl Phys 89:5243
2. Suh YS, Lazar H, Chen B, Lee JH, Mishra V (2005) J Electrochem Soc 152(9):F138
3. Kim JH, Yoon SG, Yeom SJ, Woo HK, Kil DS, Roh JS, Sohn HC (2005) Electrochem Solid-State Lett 8(6):F17
4. Sullivan JP, Tung RT, Pinto MR, Graham WR (1991) J Appl Phys 70(12):7403
5. Miura S, Tsunoda M, Takahashi M (2001) J Appl Phys 89:6308
6. Abe Y, Shinkai S, Sasaki K, Yan J, Maekawa K (2004) Jpn J Appl Phys 43:277
7. Kresse G, Hafner J (1993) Phys Rev B 47:R558
8. Kresse G, Furthmuller J (1996) Comput Mater Sci 6:15
9. Perdew JP, Chevary J, Vosko S, Jackson K, Pederson M, Singh D, Fiolhais C (1992) Phys Rev B 46:6671
10. Mukhopadhyay AB, Sanz JF, Musgrave CB (2006) Phys Rev B 73:115330
11. Mukhopadhyay AB, Sanz JF, Musgrave CB (2006) Chem Mater 18:397
12. Mukhopadhyay AB, Sanz JF, Musgrave CB (2007) J Phys Chem C 111:9203
13. Baldereschi A, Baroni S, Resta R (1988) Phys Rev Lett 61:734
14. Peressi M, Binggeli N, Baldereschi A (1998) J Phys D 31:1273
15. Franciosi A, Van de Walle CG (1996) Surf Sci Rep 25:1
16. Dong YF, Wang SJ, Chai JW, Feng YP, Huan ACH (2005) Appl Phys Lett 86:132103
17. Afanas'ev VV, Stesmans A, Chen F, Shi X, Campbell SA (2002) Appl Phys Lett 81:1053
18. Dong DF, Wang SJ, Feng YP, Huan ACH (2006) Phys Rev B 73:45302
19. Tapajna M, Harmatha L, Husekova H (2006) Solid State Electron 50:177